Mid-IR optical properties of silicon doped InP

Panah, Mohammad Esmail Aryaee; Han, Li; Norrman, Kion; Pryds, Nini; Nadtochiy, A.; Zhukov, A. E.; Lavrinenko, Andrei; Semenova, Elizaveta

Published in:
Optical Materials Express

Link to article, DOI:
10.1364/OME.7.002260

Publication date:
2017

Document Version
Publisher's PDF, also known as Version of record

Research Article | Vol. 7, No. 7 | 1 Jul 2017 | OPTICAL MATERIALS EXPRESS 2260
Optical Materials EXPRESS

Mid-IR optical properties of silicon doped InP

M. E. Aryaee Panah,[1,*] L. Han,[2] K. Norrman,[2] N. Pryds,[2] A. Nadtochiy,[3] A. E. Zhukov,[3] A. V. Lavrinenko,[1] and E. S. Semenova[1]

[1]*Technical University of Denmark, Department of Photonics Engineering, Ørsteds Plads, Building 343, DK-2800 Kgs. Lyngby, Denmark*
[2]*Technical University of Denmark, Department of Energy Conversion and Storage, Frederiksborgvej 399, Building 779, DK-4000 Roskilde, Denmark*
[3]*St. Petersburg Academic University, 8/3 Khlopina, St. Petersburg 194021, Russia*
**mesm@fotonik.dtu.dk*

Abstract: InP is one of the most important materials for optoelectronics as a direct bandgap semiconductor, which can also be regarded as a low loss alternative plasmonic material for mid-infrared (mid-IR). The InP films studied in this work were grown by metal-organic vapor phase epitaxy (MOVPE). The effect of growth conditions on the optical and electrical properties of silicon doped InP (InP:Si) in the wavelength range from 3 to 40 μm was studied. The carrier concentration of up to 3.9×10^{19} cm^{-3} is achieved by optimizing the growth conditions. The dielectric function, effective mass of electrons and plasma frequency were determined by Fourier transform infrared spectroscopy (FTIR) for different carrier density levels. The plasma frequency can be tuned effectively via doping from 18.43 to 50.5 THz. Based on the experimental results, a semi-empirical formula for the plasma frequency, as a function of carrier concentration, is derived. Comparison to other semiconductors shows superior plasmonic performance of InP:Si in terms of propagation length and surface confinement.

OCIS codes: (160.6000) Semiconductor materials; (160.4670) Optical materials; (260.3060) Infrared; (310.1860) Deposition and fabrication; (250.5403) Plasmonics.

References and links

1. S. A. Maier, *Plasmonics: Fundamentals and Applications* (Springer, 2007).
2. H. A. Atwater and A. Polman, "Plasmonics for improved photovoltaic devices," Nat. Mater. **9**(3), 205–213 (2010).
3. M. Bauch, K. Toma, M. Toma, Q. Zhang, and J. Dostalek, "Plasmon-enhanced fluorescence biosensors: a review," Plasmonics **9**(4), 781–799 (2014).
4. M. R. Philpott, "Effect of surface plasmons on transitions in molecules," J. Chem. Phys. **62**(5), 1812–1817 (1975).
5. S. Shuang, R. Lv, Z. Xie, and Z. Zhang, "Surface plasmon enhanced photocatalysis of Au/Pt-decorated TiO_2 nanopillar arrays," Sci. Rep. **6**(1), 26670 (2016).
6. J. A. Dionne, L. A. Sweatlock, H. A. Atwater, and A. Polman, "Planar metal plasmon waveguides: frequency-dependent dispersion, propagation, localization, and loss beyond the free electron model," Phys. Rev. B **72**(7), 075405 (2005).
7. J. B. Pendry, "Negative refraction makes a perfect lens," Phys. Rev. Lett. **85**(18), 3966–3969 (2000).
8. D. Rodrigo, O. Limaj, D. Janner, D. Etezadi, F. J. García de Abajo, V. Pruneri, and H. Altug, "Mid-infrared plasmonic biosensing with graphene," Science **349**(6244), 165–168 (2015).
9. S. Law, V. Podolskiy, and D. Wasserman, "Towards nano-scale photonics with micro-scale photons: The opportunities and challenges of mid-infrared plasmonics," Nanophotonics **2**(2), 103–130 (2013).
10. G. V. Naik and A. Boltasseva, "Semiconductors for plasmonics and metamaterials," Phys. Status Solidi Rapid Res. Lett. **4**(10), 295–297 (2010).
11. Y. Zhong, S. D. Malagari, T. Hamilton, and D. Wasserman, "Review of mid-infrared plasmonic materials," J. Nanophotonics **9**(1), 093791 (2015).
12. A. Boltasseva, "Empowering plasmonics and metamaterials technology with new material platforms," MRS Bull. **39**(5), 461–468 (2014).
13. K. Anglin, T. Ribaudo, D. C. Adams, X. Qian, W. D. Goodhue, S. Dooley, E. A. Shaner, and D. Wasserman, "Voltage-controlled active mid-infrared plasmonic devices," J. Appl. Phys. **109**(12), 123103 (2011).

#293433 https://doi.org/10.1364/OME.7.002260
Journal © 2017 Received 24 Apr 2017; revised 21 May 2017; accepted 21 May 2017; published 7 Jun 2017

Optical Materials EXPRESS

14. K. Yvind, D. Larsson, J. Mørk, J. M. Hvam, M. Thompson, R. Penty, and I. White, "Low-noise monolithic mode-locked semiconductor lasers through low-dimensional structures," in *Proceedings of SPIE - The International Society for Optical Engineering* (2008), 69090A.
15. N. Grote, M. Baier, and F. Soares, "Photonic integrated circuits on InP," Springer Ser. Opt. Sci. **161**, 799–840 (2017).
16. Z. Wang, B. Tian, M. Pantouvaki, W. Guo, P. Absil, J. Van Campenhout, C. Merckling, and D. Van Thourhout, "Room-temperature InP distributed feedback laser array directly grown on silicon," Nat. Photonics **9**(12), 837–842 (2015).
17. S. Learkthanakhachon, A. Taghizadeh, G. C. Park, K. Yvind, and I.-S. Chung, "Hybrid III-V/SOI resonant cavity enhanced photodetector," Opt. Express **24**(15), 16512–16519 (2016).
18. G. C. Park, W. Xue, A. Taghizadeh, E. Semenova, K. Yvind, J. Mørk, and I.-S. Chung, "Hybrid vertical-cavity laser with lateral emission into a silicon waveguide," Laser Photonics Rev. **9**(3), L11–L15 (2015).
19. S. Stephan, D. Frederic, and A. Markus-Christian, "Novel InP- and GaSb-based light sources for the near to far infrared," Semicond. Sci. Technol. **31**(11), 113005 (2016).
20. M. E. Panah, O. Takayama, S. V. Morozov, K. E. Kudryavtsev, E. S. Semenova, and A. V. Lavrinenko, "Highly doped InP as a low loss plasmonic material for mid-IR region," Opt. Express **24**(25), 29077–29088 (2016).
21. S. Adachi, "Model dielectric constants of GaP, GaAs, GaSb, InP, InAs, and InSb," Phys. Rev. B Condens. Matter **35**(14), 7454–7463 (1987).
22. D. E. Aspnes and A. A. Studna, "Dielectric functions and optical parameters of Si, Ge, GaP, GaAs, GaSb, InP, InAs, and InSb from 1.5 to 6.0 eV," Phys. Rev. B **27**(2), 985–1009 (1983).
23. H. Burkhard, H. W. Dinges, and E. Kuphal, "Optical properties of $In_{1-x}Ga_xP_{1-y}As_y$, InP, GaAs, and GaP determined by ellipsometry," J. Appl. Phys. **53**(1), 655–662 (1982).
24. A. De and C. E. Pryor, "Optical dielectric functions of III-V semiconductors in wurtzite phase," *https://arxiv.org/abs/1011.3081*.
25. A. B. Djurišić, Y. Chan, and E. H. Li, "The model dielectric function: application to GaSb and InP," Semicond. Sci. Technol. **16**(11), 902–908 (2001).
26. S. M. Kelso, D. E. Aspnes, M. A. Pollack, and R. E. Nahory, "Optical properties of $In_{1-x}Ga_xAs_yP_{1-y}$ from 1.5 to 6.0 eV determined by spectroscopic ellipsometry," Phys. Rev. B **26**(12), 6669–6681 (1982).
27. R. C. Jayasinghe, Y. F. Lao, A. G. U. Perera, M. Hammar, C. F. Cao, and H. Z. Wu, "Plasma frequency and dielectric function dependence on doping and temperature for p-type indium phosphide epitaxial films," J. Phys. Condens. Matter **24**(43), 435803 (2012).
28. H. Q. Zheng, K. Radahakrishnan, S. F. Yoon, and G. I. Ng, "Electrical and optical properties of Si-doped InP grown by solid source molecular beam epitaxy using a valved phosphorus cracker cell," J. Appl. Phys. **87**(11), 7988–7993 (2000).
29. M. M. El-Nahass, S. B. Youssef, and H. A. M. Ali, "Optical properties of sulfur doped InP single crystals," Physica A **402**, 216–223 (2014).
30. Q. H. Hua, G. P. Li, X. K. He, Q. Wang, and T. N. Sun, "Infrared reflectance study of n-type InP grown by the LEC method," Mater. Lett. **3**(3), 93–97 (1985).
31. W. G. Breiland, M. E. Coltrin, J. R. Creighton, H. Q. Hou, H. K. Moffat, and J. Y. Tsao, "Organometallic vapor phase epitaxy (OMVPE)," Mater. Sci. Eng. **24**(6), 241–274 (1999).
32. P. R. Berger, S. N. G. Chu, R. A. Logan, E. Byrne, D. Coblentz, J. Lee III, N. T. Ha, and N. K. Dutta, "Substrate orientation effects on dopant incorporation in InP grown by metalorganic chemical vapor deposition," J. Appl. Phys. **73**(8), 4095–4097 (1993).
33. C. Blaauw, F. R. Shepherd, C. J. Miner, and A. J. Springthorpe, "Silicon incorporation in InP during LP-MOCVD using disilane," J. Electron. Mater. **19**(1), 1–6 (1990).
34. A. R. Clawson, T. T. Vu, and D. I. Elder, "A comparison of IV and VI n-dopants for MOVPE-grown InP," J. Cryst. Growth **83**(2), 211–218 (1987).
35. M. A. Di Forte-Poisson, C. Brylinski, and J. P. Duchemin, "Growth of ultrapure and Si-doped InP by low pressure metalorganic chemical vapor deposition," Appl. Phys. Lett. **46**(5), 476–478 (1985).
36. Ch. Giesen, X. G. Xu, R. Hovel, M. Heuken, and K. Heime, "Silicon doping of InP grown by MOVPE using tertiarybutylphosphine," in *Proceedings of the International Conference on Indium Phosphide and Related Materials* (1997), pp. 47–50.
37. S. Leu, H. Protzmann, F. Höhnsdorf, W. Stolz, J. Steinkirchner, and E. Hufgard, "Si-doping of MOVPE grown InP and GaAs by using the liquid Si source ditertiarybutyl silane," J. Cryst. Growth **195**(1–4), 91–97 (1998).
38. M. Oishi, S. Nojima, and H. Asahi, "Silicon doping in InP grown by metalorganic vapor phase epitaxy using silane," Jpn. J. Appl. Phys., Part 2 **24**(5), L380–L382 (1985).
39. E. Woelk and H. Beneking, "Doping of InP and GaInAs during organometallic vaporphase epitaxy using disilane," J. Appl. Phys. **63**(8), 2874–2876 (1988).
40. A. R. Clawson and C. M. Hanson, "MOCVD grown Si-doped n+ InP layers for the subcollector region in HBTs," in *Proceedings of the Sixth International Conference on Indium Phosphide and Related Materials* (1994), pp. 114–117.
41. M. E. Aryaee Panah, L. Han, D. V. Christensen, N. Pryds, A. V. Lavrinenko, and E. S. Semenova, "Silicon doped InP as an alternative plasmonic material for mid-infrared," in *Proceedings of the 41st International Conference on Infrared, Millimeter and Terahertz Waves* (2016), 7758994.

Optical Materials EXPRESS

42. W. Walukiewicz, J. Lagowski, L. Jastrzebski, P. Rava, M. Lichtensteiger, C. H. Gatos, and H. C. Gatos, "Electron mobility and free-carrier absorption in InP; determination of the compensation ratio," J. Appl. Phys. **51**(5), 2659–2668 (1980).
43. C. J. Gabriel and A. Nedoluha, "Transmittance and Reflectance of Systems of Thin and Thick Layers," Opt. Acta (Lond.) **18**(6), 415–423 (1971).
44. W. H. Press, B. P. Flannery, S. A. Teukolsky, and W. T. Vetterling, *Numerical Recipes* (Cambridge University Press, 1986).
45. M. Cardona, "Temperature dependence of the refractive index and the polarizability of free carriers in some III-V semiconductors," in *Proceedings of the International Conference on Semiconductor Physics* (1960), pp. 388–394.
46. J. C. Ginn, R. L. Jarecki, Jr., E. A. Shaner, and P. S. Davids, "Infrared plasmons on heavily-doped silicon," J. Appl. Phys. **110**(4), 043110 (2011).
47. S. Law, R. Liu, and D. Wasserman, "Doped semiconductors with band-edge plasma frequencies," J. Vac. Sci. Technol. B **32**(5), 052601 (2014).
48. S. Law, D. C. Adams, A. M. Taylor, and D. Wasserman, "Mid-infrared designer metals," Opt. Express **20**(11), 12155–12165 (2012).
49. G. V. Naik, V. M. Shalaev, and A. Boltasseva, "Alternative Plasmonic Materials: Beyond Gold and Silver," Adv. Mater. **25**(24), 3264–3294 (2013).

1. Introduction

Plasmonics is a growing field within nanophotonics which deals with excitation of the collective oscillations of free charges, known as plasmons, in a conductive material, resulting in a drastically enhanced electromagnetic field in the vicinity of the material interface. Plasmons can be excited by exposing subwavelength conductive particles to an external electromagnetic field, resulting in localized plasmon-polaritons (LPP) or by coupling the external field to the oscillating charges near the surface of the material, resulting in a highly confined surface wave propagating along the interface between the conductive and dielectric media, known as surface plasmon-polaritons (SPP) [1]. High confinement of this enhanced field provides higher local optical density of states and leads to applications such as plasmon-enhanced photovoltaics [2], biosensing [3], Raman spectroscopy [4] and photocatalysis [5]. Furthermore, SPP's enable subwavelength spatial confinement of light, due to their dispersion properties. This very important property of SPP's is used in many fields including subwavelength waveguiding [6] and optical superlenses [7].

Metals such as Au, Ag and Cu are considered as traditional plasmonic materials for the visible range. However, when it comes to the mid- and far-infrared (IR) ranges, which are the hosts for many applications such as chemo-sensing [8] and thermal imaging [9], metals suffer from high optical losses and poor spatial confinement of SPP's. In addition, CMOS incompatibility of the noble metals is a challenge in the fabrication process of nanophotonic devices.

Alternative plasmonic materials such as graphene, ceramics, conductive oxides and semiconductors have been introduced to address these shortcomings [10,11]. Semiconductors play a key role in this context, owing to their high carrier mobility and low optical losses [12]. In addition, tunability of their optical properties via doping or charge depletion [13] adds an additional degree of freedom for engineering photonic device elements. InP as a direct bandgap III-V semiconductor is one of the most common materials in optoelectronic applications [14] and as a platform for photonic integrated circuits [15,16], photodetectors [17], vertical cavity surface emitting lasers (VCSELs) [18], and InP-based mid-IR light emitting diodes (LEDs) [19]. The operating wavelength of InP-based quantum well lasers is up to 2.7 μm [19]. In addition, highly doped InP can be considered as a plasmonic material with superior plasmonic properties compared to majority of other semiconductors in the mid-IR range owing to lower losses [20]. Furthermore, easy integration and compatibility with conventional III-V optoelectronic devices and their fabrication processes make InP a promising candidate as a perspective plasmonic material aiming for the mid-IR range.

Dielectric function of a material yields key information for understanding of its plasmonic behavior. Optical properties of undoped InP in ultra-violet, visible and near-IR ranges were investigated by different research groups [21–26]. Jayasinghe *et al.* [27] studied the dielectric

Optical Materials EXPRESS

function and plasma frequency of p-doped InP in the IR range. The maximum carrier concentration considered was 2.4×10^{19} cm^{-3} pertaining to a plasma wavelength of 15.4 µm. The large plasma wavelength in this case is due to the high effective mass of the holes. Zheng *et al.* [28] was able to achieve free electron concentrations as high as 1.1×10^{20} cm^{-3} in InP:Si, using molecular beam epitaxy (MBE). The electrical and optical properties were measured by the Hall-effect and photoluminescence, respectively. El-Nahass *et al.* [29] measured the absorption coefficient and refractive index of sulfur doped InP with a carrier concentration of 3×10^{18} cm^{-3} in the wavelength range of 200-2500 nm. Hua *et al.* [30] measured the IR reflectance of bulk sulfur and tin doped InP samples with the maximum carrier concentration of 1.2×10^{19} cm^{-3}, and studied the position of the reflectance minima for different carrier concentrations.

MOVPE is a powerful and flexible technology for epitaxial growth of compound semiconductors. It is widely used now due to the ability of instantaneous control over the partial pressure and flow rates of the precursor gasses which results in well-defined growth of a wide variety of semiconductor materials [31]. The free carrier concentration in the grown semiconductors is an important parameter which needs to be carefully controlled by choosing proper growth conditions such as the ratio of the precursor gasses, growth temperature and overall pressure of the growth chamber. Si is commonly used as a donor in MOVPE grown InP and the effect of growth conditions on its incorporation efficiency has been investigated [32–39]. In this regard, to the authors' best knowledge, the highest reported carrier concentration in MOVPE grown InP:Si has been reported as 2.6×10^{19} cm^{-3} [40].

In our previous works [20,41] we have shown that highly doped InP can support SPPs, and its plasmonic properties can be effectively tuned by adjusting the free carrier concentration. The aim of the present work is to provide a database of the growth conditions and mid-IR optical properties of InP:Si with different doping levels. Influence of the growth parameters, namely the precursor's ratio and the dopant's flux, on the carrier concentration and self-compensation in InP:Si, measured by the Hall-effect measurement (van der Pauw method) and time-of-flight secondary ion mass spectrometry (TOF-SIMS), is investigated. Furthermore, the dielectric function of the grown material with different carrier concentrations is determined using IR reflectance spectroscopy. The effect of the carrier concentration on the effective mass of electrons, plasma frequency and electrons plasma damping is discussed.

2. Experiment and discussion

The samples were grown on single-side polished (1 0 0) semi-insulating InP:Fe substrates in a low pressure MOVPE TurboDisc® reactor, with hydrogen (H_2) as a carrier gas, using phosphine (PH_3), trimethylindium (TMIn) and disilane (Si_2H_6) as the precursors for phosphorus, indium and silicon, respectively. The growth temperature, controlled by emissivity corrected pyrometers, was 610 °C. The carrier disk rotates with 1000 rpm inside the growth reactor chamber, transforming a laminar flow pattern of supplied precursor gasses into the circumferential flows and forms the so called boundary layer on top of the wafer surface. This boundary layer provides diffusion driven transport of precursors to the growing surface which results in uniform growth with a predictable rate. The growth conditions, namely the phosphorus to indium precursors' molar ratio and the disilane flux were adjusted, resulting in different free carrier concentrations.

Free carrier concentration of the samples was determined by Hall-effect measurements, which were carried out at room temperature using the van der Pauw method with a variable magnetic field (from zero up to 1.5 T).

Disilane is commonly used as the precursor for Si doping of MOVPE grown InP whose dissociation is described by a two-step process as

$$Si_2H_6 \rightarrow SiH_2 + SiH_4 \quad (1)$$

Optical Materials EXPRESS

$$SiH_4 \rightarrow SiH_2 + H_2 \quad (2)$$

where Si in SiH_2 will react on the surface of the epilayer and contribute to doping. At temperatures below 700 °C, the decomposition efficiency of silane (SiH_4) is very low and therefore the Si incorporation rate is mainly determined by Eq. (1). The decomposition efficiency of disilane [Eq. (1)] is proportional to the temperature up to 610 °C [36] (reported 625 °C in [33]) and is mass transport limited above that. At this point increasing the disilane flux will increase the carrier concentration up to a threshold point above which the layer morphology will be deteriorated [33]. The doping efficiency also slightly depends on the phosphine to TMIn molar ratio (V/III ratio). This proportional dependence is assumed to be a consequence of the reaction [36]

$$PH_3 + SiH_2 \rightleftarrows SiH_3PH_2 \quad (3)$$

which is dependent on the group V supply and can contribute to doping by incorporation of Si from SiH_3PH_2 into the growing epilayer.

The flux of TMIn, which is supplied from a solid source through a bubbler, is calculated as [31]

$$F_{\mathrm{TMIn}} = \frac{\alpha F_{\mathrm{hydrogen}} p_{\mathrm{TMIn}}}{\left(p_{\mathrm{bubbler\ total}} - p_{\mathrm{TMIn}}\right)} \quad (4)$$

where P_{TMIn} is the saturated vapor pressure of TMIn in the bubbler, F_{hydrogen} is the hydrogen flux, $p_{\mathrm{bubbler\ total}}$ is the total overpressure within the bubbler (500 mbar) and α is the efficiency of the bubbler which can be assumed to be unity with a good accuracy [31]. The molar flux of TMIn can readily be calculated using F_{TMIn} and the ideal gas law. Molar fluxes of PH_3, which is supplied directly from a gas source, as well as disilane, which is supplied as a 200 ppm diluted gas in hydrogen, can also be calculated using the ideal gas law.

All the samples were grown at 610 °C and an overall chamber pressure of 60 Torr. Table 1 summarizes the growth conditions, the resulting carrier concentration and mobility of the samples. Figure 1 shows the carrier concentration versus the disilane to TMIn molar flux ratio for two groups of samples with different V/III molar ratios. The carrier concentration is proportional to the disilane to TMIn molar flux ratio up to a threshold point where the excess Si precipitates on the surface of the sample and deteriorates it (Fig. 2). As explained above, a higher V/III ratio results in slightly higher carrier concentrations.

In order for the Si atoms to contribute as donors they should be incorporated into the sub-lattice of the IIIrd group, but in some cases, Si atoms may be incorporated to the sub-lattice of the Vth group and act as acceptors, or sit in interstitial sites of the crystal. This phenomenon, which is one of the barriers against high doping of InP, is known as self-compensation [42].

The concentration of Si atoms was determined using TOF-SIMS and subsequently compared to the free carrier concentration in the grown samples. In this regard a reference sample was ion implanted with a known amount of ^{28}Si in order to calibrate the TOF-SIMS response to the concentration. TOF-SIMS depth profiling analysis was performed on the grown InP:Si samples. The erosion rate was calculated to be 15.6 nm/min by measuring the resulting crater depth for the thickest epilayer using a Dektak 3030 surface profile measuring system (Sloan Technology Corp.) and relating the depth to the sputter time. The Si concentrations were extracted from depth profiles through the entire epilayer and the error bars are typically based on 50–100 in-depth measuring points. The TOF-SIMS measurement results with associated error bars are presented in Fig. 1. For all samples, the difference between the Si concentration measured by TOF-SIMS and the donors concentration measured by the Hall method is smaller than the error bars, which shows that the compensation ratio

Optical Materials EXPRESS

(ratio of the ionized acceptors to the ionized donor concentration) is smaller than the measurement limit.

Table 1. Growth parameters and the electrical properties of the samples

Sample	PH_3 flux × 10^{-2} [mol/min]	TMIn flux × 10^{-5} [mol/min]	Disilane flux × 10^{-9} [mol/min]	Thickness [nm]	Free carrier concentration [× 10^{19} cm^{-3}]	Mobility [cm^2/V.s]
1	1.534	6.163	0.769	485	0.35	1490
2	1.096	7.066	2.696	570	0.86	723
3	1.096	7.066	4.623	533	1.71	893
4	1.096	7.066	5.392	531	1.94	901
5	1.096	7.066	6.164	536	2.35	480
6	1.534	6.024	5.253	475	2.7	821
7	1.534	6.024	6.935	651	3.09	689
8	1.534	6.163	7.319	516	3.39	749
9	1.534	6.024	7.319	503	3.87	671

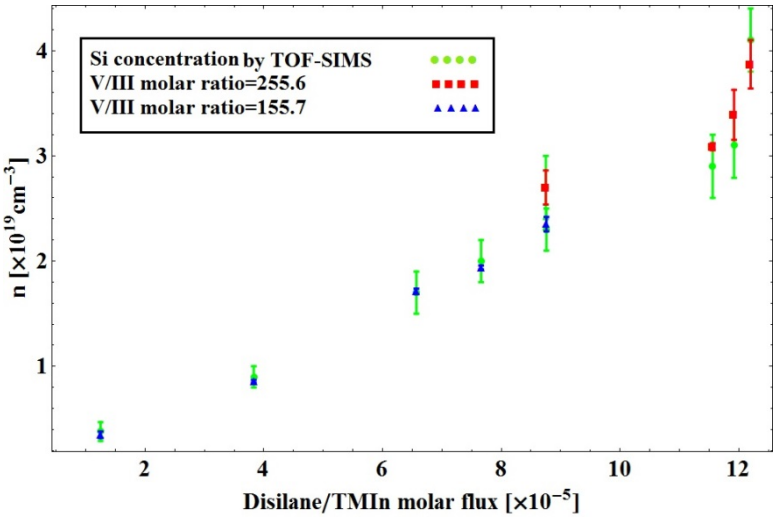

Fig. 1. Carrier concentration versus Si_2H_6/TMIn molar ratio for two different V/III molar ratios, together with the TOF-SIMS measurement results.

Fig. 2. Differential interference contrast (DIC) optical microscope image of the deteriorated surface of a sample with Si_2H_6/TMIn molar ratio equal to 15.27 × 10^{-5}.

3. Dielectric function

In order to use a material for optical applications, one needs to know its dielectric function which defines the material dispersion in the wavelength range of interest. In this section, the

Optical Materials EXPRESS

dielectric function of the grown samples at different carrier concentrations is determined after characterization of the material in the mid-IR range.

The reflectance spectra of the samples under normal incidence were calculated using the intensity transfer matrix method [43]. The purpose of this method is to ignore the Fabry-Perot interference fringes originating from the thick substrate while the interference fringes from the epilayer are retained. The Drude-Lorentz (D-L) model was applied as the dielectric function for both doped and semi-insulating InP, where the Drude term accounts for the contribution of free electrons and the Lorentzians account for the contribution of phonons to the optical dispersion of the material:

$$\varepsilon(\omega)=\varepsilon_{\infty}\left(1-\frac{\omega_p^2}{\omega^2+i\omega\gamma}\right)+\sum_j\frac{S_j\omega_{f,j}^2}{\omega_{f,j}^2-\omega^2-i\omega\Gamma_j} \tag{5}$$

Here ε_{∞} , ω_p , γ and i are the high-frequency dielectric constant, plasma frequency, electrons plasma damping and imaginary unit ($\sqrt{-1}$) respectively. S_j , $\omega_{f,j}$ and Γ_j are the strength, resonance frequency and damping for the jth Lorentzian oscillator respectively, describing phonon absorption at frequency $\omega_{f,j}$. In the wavelength range under consideration (>3 μm), the energy of photons is less than the smallest bandgap energy of InP, 1.35 eV [21], therefore the role of interband transitions is negligible.

The reflectance spectra of the samples at near-normal incidence (12°) were measured from 3 to 40 μm, using a VERTEX 70 FTIR spectrometer from Bruker. The measurements were repeated on five different points on each sample and normalized to the reflection from the aluminum mirror of the sample holder.

Table 2. Fitted parameters of the D-L dielectric function

Sample	ω_p [THz]	γ [THz]	$\omega_{f,1}$ [THz]	Γ_1 [THz]	S_1
1	18.43	1.45	9.09	0.081	2.18
2	28	1.91	9.09	0.032	1.52
3	37.12	2.85	9.08	0.04	1.91
4	38.17	2.36	9.12	0.07	3.66
5	39.87	3.45	9.07	0.056	1.89
6	41.41	1.38	9.08	0.036	1.52
7	43.57	1.71	9.11	0.082	2.86
8	45.6	1.09	9.08	0.045	1.72
9	50.5	3.49	9.12	0.082	2.52

Afterwards, the calculated reflectance spectra were fitted to the experimental data in order to find the parameters of the D-L dielectric functions. The fitting was done using the Levenberg-Marquardt algorithm [44], weighted with the inverse of the standard error for each measured point. This procedure was first carried out for the bare InP:Fe substrate and then the fitted parameters of the substrate were used to calculate and fit the reflectance from the grown samples. In all cases, ε_{∞} is considered to have a constant value equal to 9.55 [42]. Figure 3 shows the measured and the fitted reflectance spectra of the bare semi-insulating InP:Fe substrate. The rough backside of the substrate and also optical losses of the InP:Fe, diminish the reflection from backside of the samples. Table 2 summarizes the fitted parameters of all the grown InP:Si epilayers.

Optical Materials EXPRESS

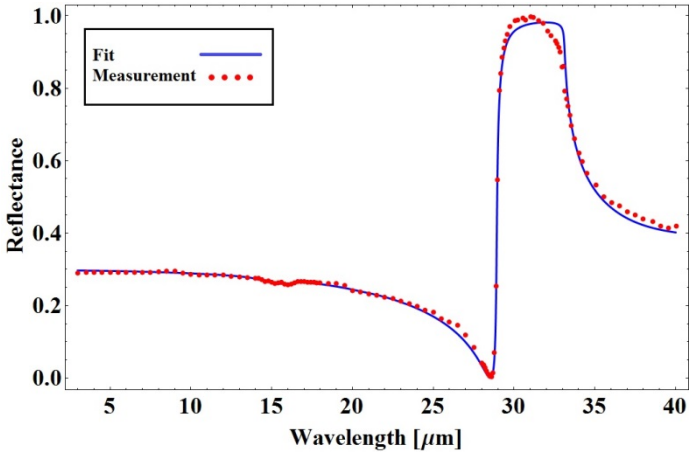

Fig. 3. Measured and fitted reflectance spectra of the bare InP:Fe substrate.

Figure 4 shows the reflectance spectra of the grown samples. As it can be seen from the figure, in case of highly doped InP, only one Lorentzian term corresponding to a transverse optical (TO) phonon line is pronounced and others are overshadowed by the plasma resonance. Based on the retrieved parameters of the D-L model and Eq. (5), we plotted in Fig. 5 the real and imaginary parts of the permittivity of the samples. The plasma wavelength of the samples varies from 5.93 μm (sample 9) to 16.26 μm (sample 1) that shows the drastic tunability of plasmonic properties of InP via doping.

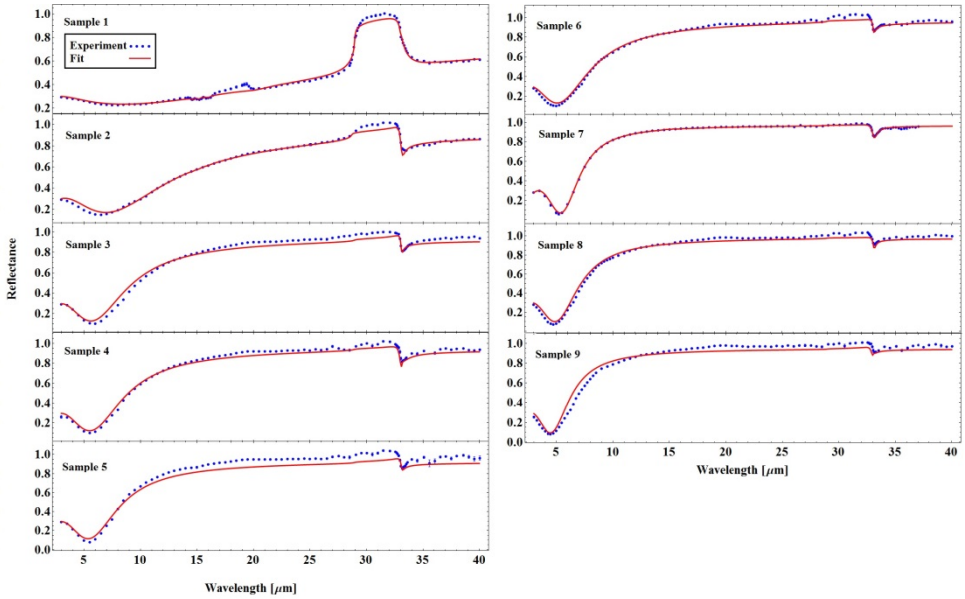

Fig. 4. Measured and fitted reflectance spectra of the grown samples.

Optical Materials EXPRESS

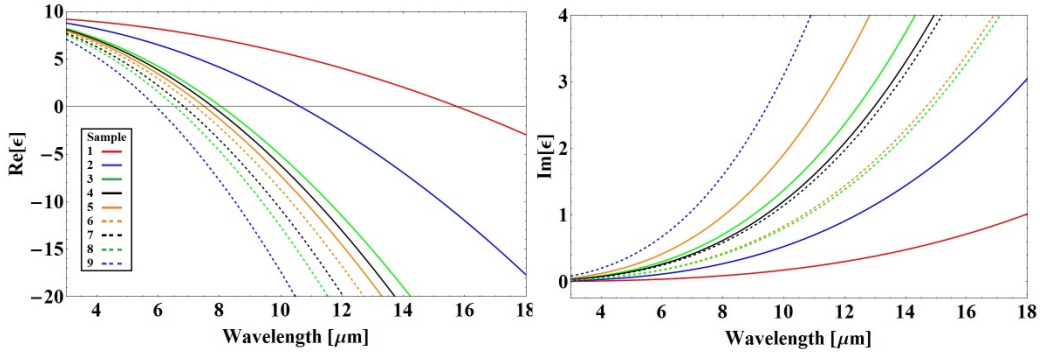

Fig. 5. Real and imaginary parts of the permittivities, from Table 2.

Figure 6 shows the retrieved plasma frequency versus the carrier concentration. The theoretical plasma frequency was calculated according to [1] as

$$\omega_p = \sqrt{\frac{ne^2}{\varepsilon_\infty \varepsilon_0 m^*}} \tag{6}$$

where n, e, ε_0 and m^* are the free electron concentration, electron charge, vacuum permittivity and effective mass of electrons, respectively. The theoretical value of m^* for n-type InP proposed in [45] is used to calculate ω_p.

Basing on the experimental results, we derived a semi-empirical formula for the plasma frequency of InP:Si as a function of the free carrier concentration (n) in the range between 0.35 to 4×10^{19} cm^{-3}:

$$\omega_p = \sqrt{An\left(1 - \frac{B}{1.344 - Cn^{\frac{1}{3}}}\right)} \tag{7}$$

where $A = 918.43\,m^3/s^2$, $B = 3.7 \times 10^{14}$, $C = 6.6 \times 10^5$ m and the units for n and the resulting ω_p are in m^{-3} and Rad/s, respectively. Here the term in parenthesis accounts for the changes in the band structure of InP, when it is highly doped with Si. ω_p calculated from Eq. (7) is also presented in Fig. 6.

Optical Materials EXPRESS

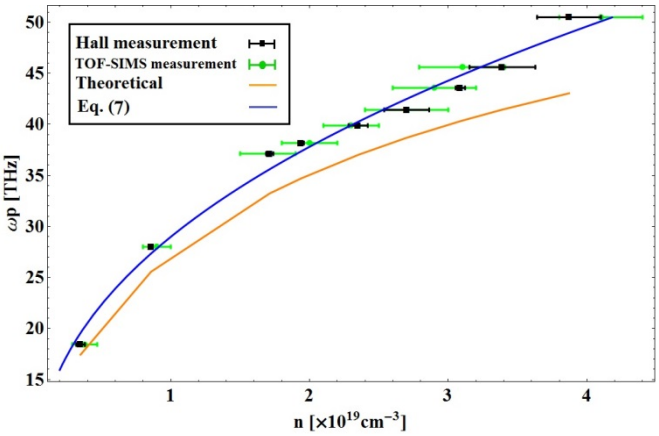

Fig. 6. ω_p versus carrier concentration from Hall and TOF-SIMS measurements together with the empirical and theoretical values.

Figure 7 shows the effective mass of electrons as a function of the carrier concentration calculated from Eq. (6) using the fitted values for ω_p versus the theoretically calculated effective mass [45]. The discrepancy between the fitted and theoretical values for ω_p in Fig. 6 can be attributed to the flaws in the theoretical formula for m^*, for example the effect of non-parabolicity of the conduction band [45], together with the fitting errors and also the errors in the Hall measurements. These sources of error also explain the discrepancies in Fig. 7. Fluctuations in the values of γ with respect to the free carrier concentration (Table 2) are correlated with the fluctuations in the mobility values measured by the Hall-effect (Table 1).

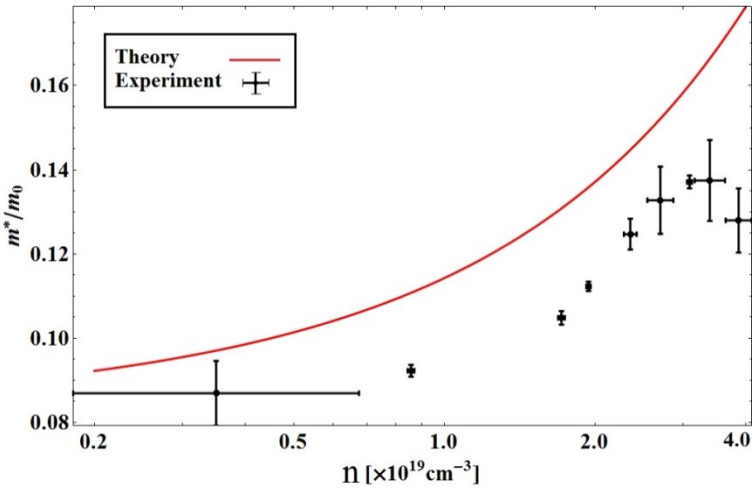

Fig. 7. Effective mass of electrons in InP:Si as a function of the carrier concentration.

4. Comparison to other semiconductors

In order to compare the mid-IR plasmonic properties of InP:Si to other semiconductors whose data are available in the literature, we have chosen the following compositions: p-doped Si, n-doped Si [46], n-doped InSb [47] and n-doped InAs [48] with plasma wavelengths close to sample 9 (5.93 μm).

The propagation length of surface plasmons L_p, is given by

Optical Materials EXPRESS

$$L_p = \left(2\,\mathrm{Im}\left[k_{spp}\right]\right)^{-1} \tag{8}$$

where $k_{spp} = k_0\sqrt{\frac{\varepsilon_m\varepsilon_d}{\varepsilon_m+\varepsilon_d}}$ is the wavevector of surface plasmons at the interface between dielectric and conductor materials with permittivities ε_d and ε_m, respectively. The localization (confinement factor) in air δ_d and in doped semiconductor δ_m are given by

$$\delta_{d/m} = \mathrm{Re}\left[\left(2\pi\sqrt{k_{spp}^2 - \varepsilon_{d/m}k_0^2}\right)^{-1}\right] \tag{9}$$

The total SPP localization is defined as $\delta_{spp} = \delta_d + \delta_m$. Figure 8 shows the propagation lengths of surface plasmons, their localization, and figures of merit (FOMs) for sample 9 compared to other semiconductors. We use two figures of merits defined in [49] as

$$\mathrm{FOM}_1 = L_p / \delta_{spp} \tag{10}$$

$$\mathrm{FOM}_2 = \mathrm{Re}(\varepsilon)^2 / \mathrm{Im}(\varepsilon) \tag{11}$$

in order to quantify the tradeoff between the confinement and propagation losses.

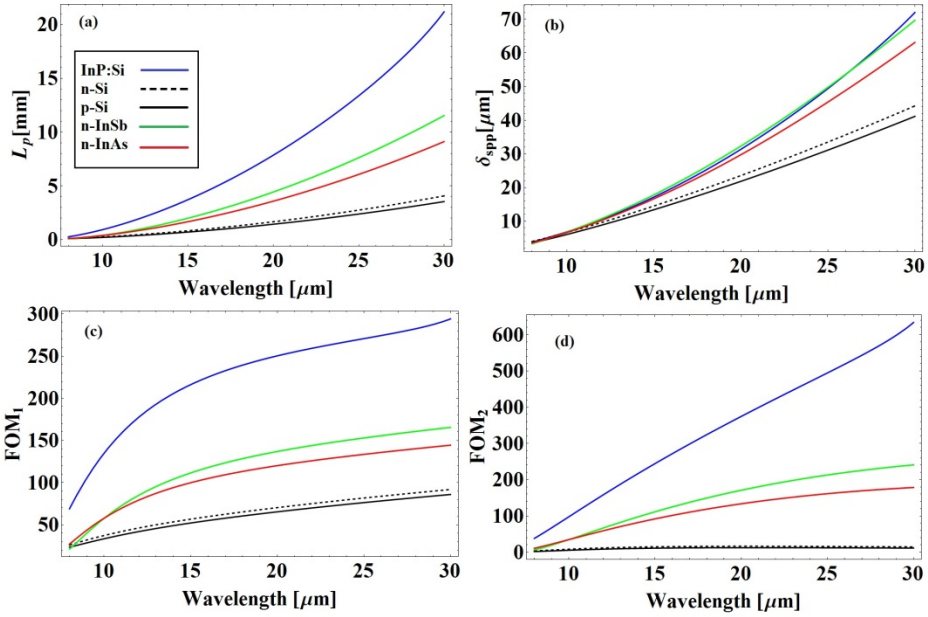

Fig. 8. (a) Propagation length, L_p, (b) localization, δ_{spp}, (c) figure of merit, L_p/δ_{spp} and (d) figure of merit $\mathrm{Re}(\varepsilon)^2/\mathrm{Im}(\varepsilon)$, for sample 9 ($\lambda_p = 5.93$ µm) in comparison with other doped semiconductors: n- ($\lambda_p = 5.54$ µm) and p-doped Si ($\lambda_p = 5.90$ µm) [46], n-InSb ($\lambda_p = 6.84$ µm) [47], and n-InAs with $\lambda_p = 6.3$ µm [48].

From Fig. 8 (a) and (b), we can see that the SPP propagation length in InP:Si is higher than in other semiconductors owing to the lower losses, and the localization of SPP's is among the others and is very close to that of n-InSb. Both FOM_1 and FOM_2 which quantify the tradeoffs between localization and propagation length, are higher for InP:Si. In

Optical Materials EXPRESS

comparison to noble metals, in the mid-IR range, both real and imaginary parts of the permittivity of InP:Si are two orders of magnitude smaller which leads to better confinement of SPPs in expense of a shorter propagation length. Nevertheless, tuanability of the plasma wavelength and damping is a very important feature of semiconductors which cannot be achieved in metals.

5. Conclusion

We have studied InP:Si samples grown by MOVPE. In particular, the effect of the growth conditions, namely the dopant flow rate and the V/III ratio, on the free carrier concentration has been studied. Using the optimal growth conditions, the maximal free carrier concentration of 3.9×10^{19} cm^{-3} is achieved. The total concentration of Si atoms, measured by TOF-SIMS, was compared to the free carrier concentration, measured by the Hall technique, and it was found that the compensation ratio in the grown samples is smaller than the measurement error. Reflectance of the samples in 3-40 μm wavelength range has been measured using FTIR, and used to retrieve the dielectric function of InP:Si by curve-fitting. The maximum plasma frequency is found to be 50.5 THz. Using the fitted plasma frequency, the effective mass of electrons is determined for different carrier concentrations. The semi-empirical Eq. (7), which accounts for the changes in the band structure of the InP upon Si doping, can be used to estimate realistic values for ω_p versus carrier concentration in the range between 0.35 to 4×10^{19} cm^{-3}.

Owing to its lower losses, InP:Si has higher figures of merit, which quantify the tradeoff between SPP confinement and propagation length, in comparison to the other doped semiconductors with a similar plasma frequency, whose data are available in the literature.

This paper provides information about the electrical and the optical properties of InP:Si and the MOVPE growth guidelines to be used for design and fabrication of optoelectronic and plasmonic devices.

Funding

FP7-PEOPLE-2013-IRSES project HyMeCav (No. 612564).

Acknowledgments

The authors would like to thank Alexander Huck for proofreading the manuscript.